TÜBİTAK

Turkish Journal of Physics

http://journals.tubitak.gov.tr/physics/

Research Article

Turk J Phys
(2013) 37: 219 – 228

doi:10.3906/fiz-1208-8

Development and utilization of a retarding analyzer for field emission investigation of LaB_6/W emitter

Ahmed A. A. AL-TABBAKH,* Mahendra A. MORE, Dilip S. JOAG
Department of Physics, Center for Advanced Studies in Material Science and Condensed Matter Physics, University of Pune, Pune, India

Received: 16.08.2012 • **Accepted:** 27.12.2012 • **Published Online:** 19.06.2013 • **Printed:** 12.07.2013

Abstract: A cold field emission from LaB_6/W-coated cathodes has been investigated with a high-accuracy and low-cost retarding field analyzer instrument. Guidelines are provided for measurements of Fowler–Nordheim (FN) characteristics and total energy distributions using a single set-up and direct detection technique to address presumed shortages in sophisticated instrumental requirements for integral investigation. Electron emission from LaB_6 nanoprotrusions, deposited on a tungsten microtip, was successfully investigated. Results emphasize a metallic behavior of the emitter in accordance with the FN theory. No size effects were observed for protrusions of 300 nm in radii.

Key words: Field electron emission, Fowler–Nordheim theory, total energy distribution, retarding field analyzer

1. Introduction

Field electron emission sources are the most advanced cold electron cathodes used in scanning electron microscopes and electron beam lithography systems due to their advantageous properties of low operating voltages, low energy spread, and high brightness [1–4]. Understanding field emission characteristics is essential for the development of new cathode materials, which has been the target of many research groups around the globe. The limited budgets and the high cost of the characterization tools have restrained many researchers from investigating their candidate materials and have restricted the parallel development of new cathodes. It is therefore aimed to provide an integrated description of a characterization tool with which a field emission investigation is possible with high accuracy and relatively low cost. A simple configuration similar to the retarding field analyzer used by Van Oostrom has been optimized, fabricated, and utilized for combined Fowler–Nordheim (FN) and quantitative total energy distribution (TED) measurements [5]. While the TEDs are highly sensitive to the measurement parameters, a description of the instrumental set-up and the device performance are presented. Calibration of the device using a lanthanum hexaboride cold cathode and measurements of the FN plot and the TED from a nanoprotrusion of the same material are also presented. For field emission studies from different morphologies of LaB_6 emitters, one may refer to other studies [4,6–8].

Field emission from metals, as explained by Fowler and Nordheim, occurs as electron tunneling from bound states [9]. The field required for an appreciable tunneling current is in the order of 3×10^7 V/cm. The tunneling current (I) is described by the FN equation as:

*Correspondence: tabbakh2003@yahoo.com

$$I = 1.54 \times 10^{-6} \ \frac{\beta^2 V^2}{\varphi\, t^2(y)} \ \exp\left[-6.8 \times 10^7 \frac{\varphi^{\frac{3}{2}}\ f(y)}{\beta V}\right], \tag{1}$$

where $t(y)$ and $f(y)$ are slowly varying functions having fairly constant values close to unity. V is the applied voltage, φ is the average work function of the emitter, and β is the field enhancement factor at the emitter surface. The FN plot ($\log\left(I/V^2\right)$ versus $10000/V$) is linear for a wide range of emitters with a slope given by Eq. (2):

$$m_{FN} = -2.9669 \times 10^3 \ \frac{\varphi^{3/2}}{\beta}\, s(y), \tag{2}$$

where $s(y)$ is another slowly varying function. Details of the FN equation and the related parameters are available elsewhere [5]. The TED has been calculated by Young and in an early work reviewed by Gadzuk and Plummer [10,11]. For infinite analyzer resolution, the TED exhibits a vertical step at the work function energy (near the Fermi level of the emitter) and an exponential decrease at higher energies (below the Fermi level). For finite resolution of the analyzer the low-energy step exhibits a less steep behavior of Gaussian shape. Nevertheless, the work function is obtained from the infliction point where the distribution slope changes sign. The position of the infliction point does not depend on the energy resolution of the analyzer [12].

2. Design, optimization, and calibration of the instrument

2.1. Single configuration, multiple utilizations

The configuration of the device, which is generally similar to that used by Van Oostrom in 1966 and by Latham and Mousa in 1986 [5,13] (mentioned hereafter as the retarding field analyzer), is depicted in Figure 1. The main feature of the retarding field method is that the resolving power of the analyzer is independent of its size as long as its geometry is conserved. The combination of the electrodes' geometries, their separations, and the operating voltages differs from the original device depending on our new utilization. The retarding analyzer (RA) is composed of an anode, a lens electrode, a shield, and a Faraday cup. The anode is a cylindrical electrode with a length-to-radius ratio of 1.5 and a phosphorous layer coated on the base to serve as a screen for the field emission pattern and to enhance the electrons' collection of the anode. A 1-mm aperture is made at the center of the anode. The apertures on the lens electrode and the shield are 2 mm and 4 mm, respectively. The Faraday collector is a half-hemisphere, 13 mm in radius, highly smoothed and coated with a high work function material to enhance electron collection and reduce secondary emission. The present configuration is used for FN characteristic measurements (current–voltage characteristics) by placing the electron emitter near the center of the anode entrance, maintaining it at varying negative potentials of a few kilovolts. The emission current is collected from all the electrodes to an electrometer for each value of the cathode potential. The field emission pattern is simultaneously recorded from the phosphorous screen through a view port in the vacuum chamber.

In quantitative TED measurements the device electrodes are connected in a certain combination, as shown in Figure 2. The anode is used to generate the required electric field for the electron emission as high positive voltage with respect to ground voltage applied on this electrode. The RA works as a high-pass filter for the field-emitted electrons. A retarding field is generated between the anode and the lens electrode so that only electrons having energies higher than the field potential pass to the final electrode, the Faraday cup. The lens (which is kept at negative potential with respect to ground) maintains a strong focusing effect and the electrons'

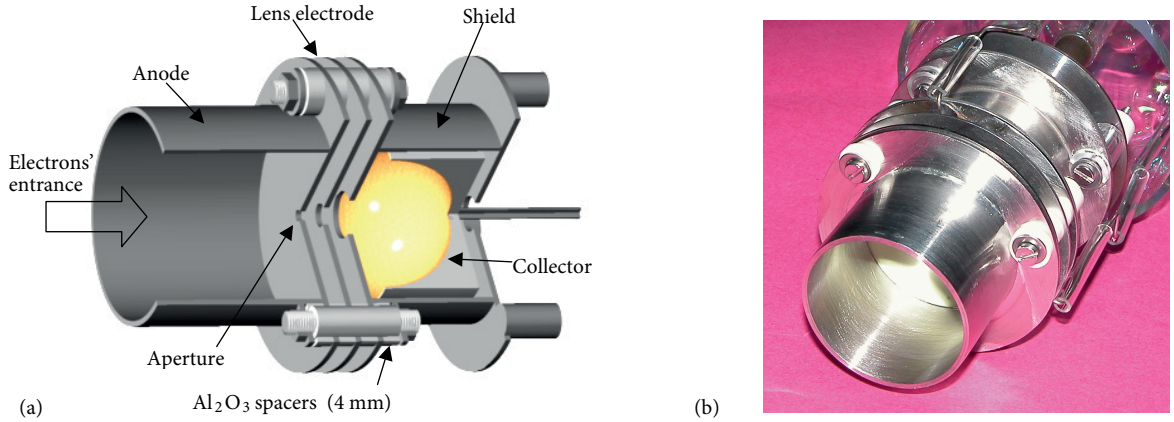

Figure 1. (a) The 3-dimensional configuration of the retarding analyzer: a cross-section. (b) The assembled analyzer.

beam achieves a crossover near the center of the collector. As a result, a perpendicular incidence of the electrons occurs and electrons' total energies are analyzed. The shield electrode is connected to ground. In the TED measurements, electrons from the aperture current are being analyzed and this current is obviously a small fraction of the total emitted current, depending on the distance between the emitter surface and the aperture. The aperturing ratio is thus defined as the ratio of the transmitted current to the collector to the total emission current. Despite the fact that a low ratio is encountered due to the high magnification of the field electron microscope (10^5), currents in the picoampere range are detectable with a high-precision picoammeter. Proper shielding is required to maintain high precision measurements and to improve the signal-to-noise ratio. This is achieved by the shield electrode, which eliminates the contribution of the off-beam electrons, and by using doubly shielded coaxial cables in the electric circuit. The sensitivity of measurement depends on the resolution of the analyzer and is further improved with the pre-retardation of electrons while maintaining a focusing effect [14,15]. It has been shown that the defocusing during deceleration could efficiently be minimized with the help

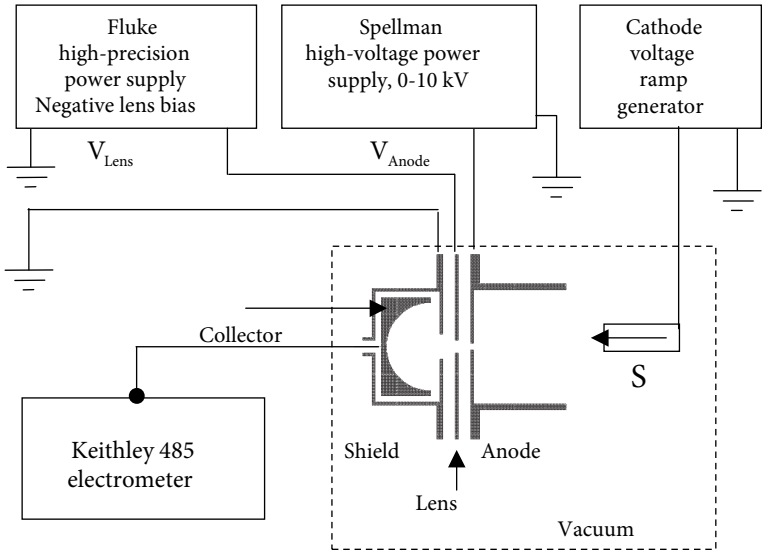

Figure 2. The electric circuit diagram for the retarding curves' measurement. S refers to the emitter specimen position.

of an electrostatic lens, and this leads to the improvement of the sensitivity of measurement [16]. The analyzer performance depends mainly on the pre-retardation of electrons (see Section 2.2). Pre-retardation will also ensure a minimal secondary emission from the surface of the collector. The output signal of the measurement is the collector current versus the emitter bias, which is the integral of the TED. This will be further illustrated below.

2.2. Resolution of measurements and modes of operation

The resolution of the analyzer is the ratio of the full width at half maximum (FWHM; ΔE) of the TED to the tuning energy (E_o) of the analyzer. E_o usually takes the practical value of the energy at which a maximum fraction of electrons transmits to the collector (i.e. the energy at which the TED peaks). There are 2 modes of operation adopted in measuring TEDs [15–18]:

a. Constant relative resolution mode ($\Delta E/E_o = const.$)

   Electrons enter the analyzer with their own energy or energy decreased by a constant amount of pre-retardation while the tuning energy of the analyzer is swept from one end of the spectrum (the range of energy to be analyzed) to the other. The transmission condition between the electron emitter and the analyzer is constant. However, this method was found to be inconvenient for quantitative spectrum analysis at low energies because the resolution becomes too high, which spoils the signal-to-noise ratio [17].

b. Constant absolute resolution mode ($\Delta E = const.$)

   This is known as constant energy mode. Electrons are decelerated by variable amounts so as to adjust their energies to the fixed tuning energy E_o of the analyzer. Absolute resolution remains unchanged in this mode, which offers better conditions for quantitative analysis, while the transmission conditions are varying during the process. Difficulty lies in proper electron optics design, which may be achieved by using a zoom lens whose function is to focus at a fixed position on an object of fixed energy and position, in spite of the fact that the energy of the image is varying.

   The second mode of operation is being adopted in the present measurements.

2.3. Direct detection technique

The output signal of the analyzer is the collector current versus the emitter bias (i.e. the number of electrons passing to the collector at each energy step). The produced graph is known as the retarding curve. A first derivative of the retarding curve produces the TED of the electrons. Electronic modulation and synchronous detection, or the phase-sensitive detection technique, yields the first derivative of the signal (i.e. TED) if the amplitude of the modulation signal is made adequately small [19]. If the sensitivity of detection is restricted by a low signal-to-noise ratio, then the signal amplitude cannot be made small to afford the modulation requirements. Therefore, the first derivative (the TED) is not necessarily determined [20]. To avoid this drawback, a direct detection technique, averaging over consecutive sweeps of the integral signal and numerical differentiation procedures, has instead been incorporated to determine the energy distributions of the field-emitted electrons.

2.4. Optimization of the analyzer operating parameters

The electrons' trajectories inside the analyzer have been simulated and investigated with the help of the electron optics SIMION 3D (version 7.0) design program. The parameters of the analyzer geometry were simulated based on the experimental requirements, and the lens-to-anode voltage (V_L/V_A) ratio was investigated so as to fulfill the optimum electron trajectory where the electron beam undergoes a crossover near the center of the collector. Figure 3 shows 3 different modes of trajectories according to the V_L/V_A ratio. By increasing the V_L/V_A ratio (as shown in Figures 3a–3c), electrons start reflecting backwards and get collected by electrodes other than the Faraday cup. The analyzer simulation results show that displaced electrons from the optical axis of the lens are subjected to higher lens effect due to the curvature of equipotential surfaces of the retarding potential. Therefore, a full retardation of monoenergetic electrons still requires a distinct change in the lens potential. Practically, off-axis electrons reflect at lower retarding potential than on-axis electrons. The finite resolution of the analyzer could therefore be attributed to this effect of electron retardation (i.e. a gradual transference from optimum trajectory to full retardation) in addition to the inherent energy spread of the field-emitted electrons. The optimum V_L/V_A ratio estimated from the SIMION 3D (version 7.0) design program was found equal to 0.0042.

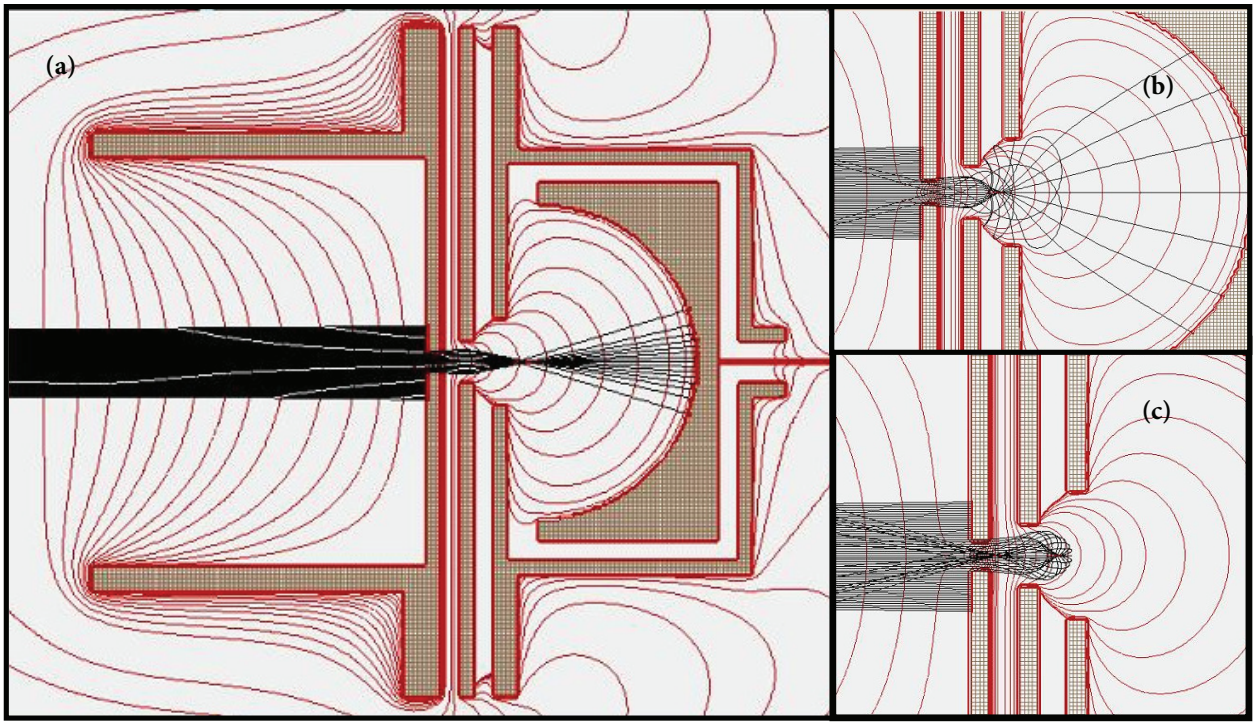

Figure 3. The simulation of the electrons' trajectories inside the analyzer. (a) Optimum trajectory with beam crossover near the center of the collector. (b) Partial beam retardation. (c) Full beam retardation.

2.5. Calibration of the retarding analyzer

Calibration is based on maximizing the collector current (I_C) by varying the V_L/V_A ratio at constant anode and emitter potentials. The emitter is negatively biased with a potential slightly higher than the work function of the collector to ensure collection of electrons at the collector surface. Figure 4 shows calibration curves at

3.4-kV anode potential for 2 values of emitter bias. The 3 distinct regions of the curves (regions a through c) could be attributed to the trajectory modes shown in Figure 3. The curves peak (region a) when optimum trajectories take place and a beam crossover at the center of the collector is achieved. Region a in Figure 4 is attributed to the optimum electron trajectory of Figure 3a, whereas region b is associated with the full retardation mode (Figure 3c). The small decrease in I_C in region c prior to acquiring a maximum (in region a) is probably due to charging effect when the focusing of electrons occurs at the surface of the collector. In this case, all electrons are expected to be collected from a very small area of the collector surface. This may promote charging effect and lead to the apparent decrease in I_C. This effect is less prominent at lower currents (see Figure 5). The curve maximum shifts to higher lens potential due to the increase in the electrons' energy at higher cathode bias. This shows that the V_L/V_A ratio does not remain constant during the TED measurement, which is in agreement with the sweeping mode of the analyzer (the constant absolute resolution) [15–18]. For further verification of this, calibration curves are now measured for different values of anode potential and constant emitter bias. Figure 5 shows that similar features of the curves are observed, but the curve maximum is independent of the anode bias. This emphasizes that anode potential is exploited for electron emission (i.e. deformation of potential barrier at the surface of the emitter) and exerts no effect on electrons' energies. In addition, the anode potential is responsible for the strong retarding potential inside the analyzer.

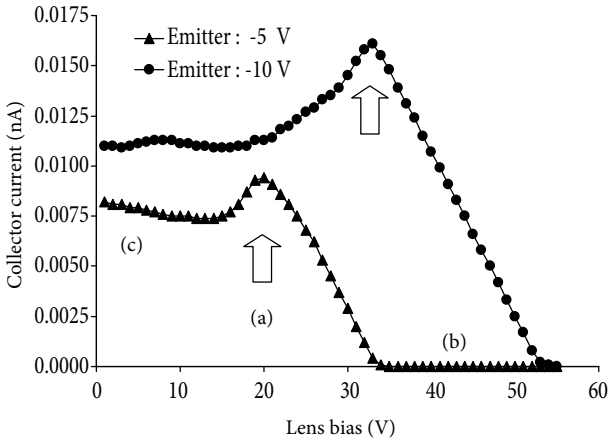

Figure 4. Calibration curve for the retarding analyzer at 2 different values of emitter bias. Region a: optimum beam trajectory. Region b: full beam retardation. Region c: weak lens effect and small charging effect.

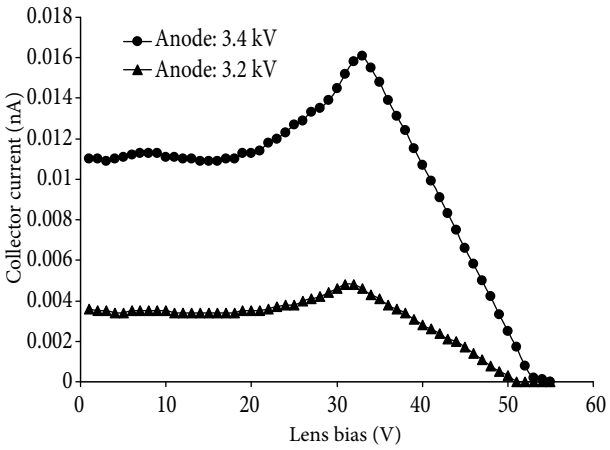

Figure 5. Calibration curves for different values of anode bias emphasizing the mode of operation of the analyzer.

The optimum values of the V_L/V_A ratio, investigated for varying emitter potentials and constant anode bias, are plotted in Figure 6. A linear dependence of the V_L/V_A ratio on cathode bias is obvious from the fitting equation (y = 0.44x – 4.2). Extrapolation of the linear fit to zero lens voltage leads to an intercept with the ordinate (the cathode bias). Recalling that electron emission entails no supply of energy to the tunneling electrons, the intercept of Figure 6 provides the work function value of the collector surface, which is equal to 4.2 eV. This value has been verified directly by measuring the emitter bias at the threshold value of I_C and zero lens potential ($V_L = 0$). The emitter bias was found equal to –4.208 V, which is equal to the work function of the collector.

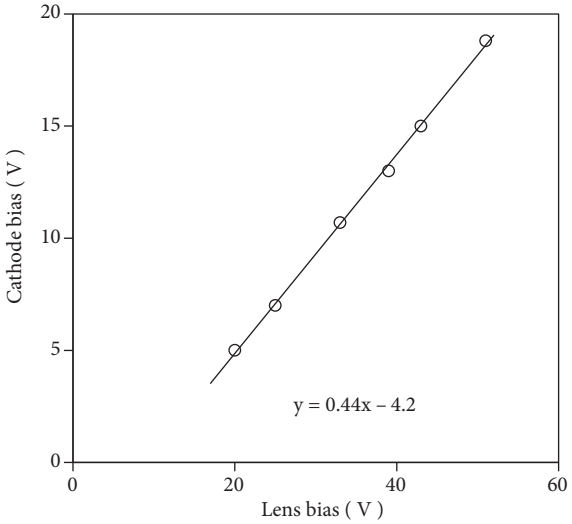

Figure 6. Work function of the collector determined from the calibration curve of the analyzer. Inset equation: y is the cathode bias and x is the lens bias. At x = 0, the cathode bias refers to the work function of the collector.

3. Field emission investigation of LaB_6/W emitter

A thick, homogeneous layer of LaB_6 has been deposited on a chemically etched tungsten (W) microtip by an optimized pulsed-laser deposition technique. A thickness of 1 μm has been reported for this deposition [21]. The surface morphology was investigated with a scanning electron microscope (JEOL 6360A). High magnification scanning electron micrographs (SEMs) (Figure 7) show the presence of protrusions with radii of less than 300 nm, from which electron emission was anticipated due to the field enhancement effect. The field emission pattern, recorded from the anode phosphorous screen, alongside the current–voltage (I–V) characteristics and the corresponding FN plot are depicted in Figure 8. The 2 bright spots in the emission pattern are related to emission from the 2 protrusions shown in the SEMs. The exponential behavior of the I–V plot and the linear FN plot signify the metallic character of the emitter. From the slope of the FN plot (–1.47), the work function

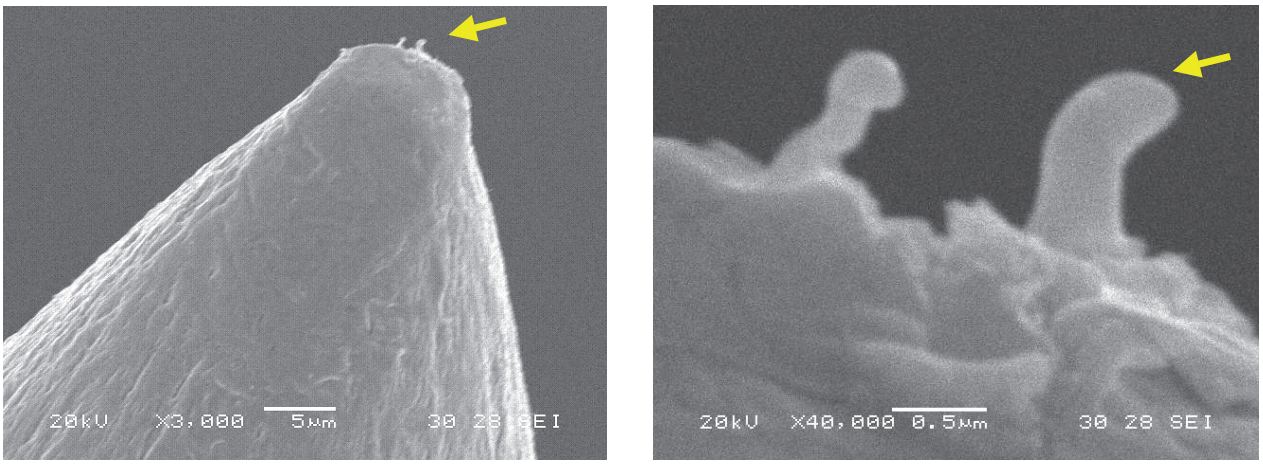

Figure 7. Scanning electron micrographs of LaB_6/W emitter synthesized by pulsed-laser deposition on tungsten microtip. The arrows point to the LaB_6 nanoprotrusions.

of the emitter (2.6 eV), and the slope equation (Eq. (2)), it is possible to estimate the enhancement factor (β) to be 8461.4 cm^{-1}. This value corresponds to a radius (r) of 236 nm calculated iteratively for $s(y) = 0.916$ (assuming $\beta = 1/ar$ and $a = 5$ for the hemispherical emitter surface).

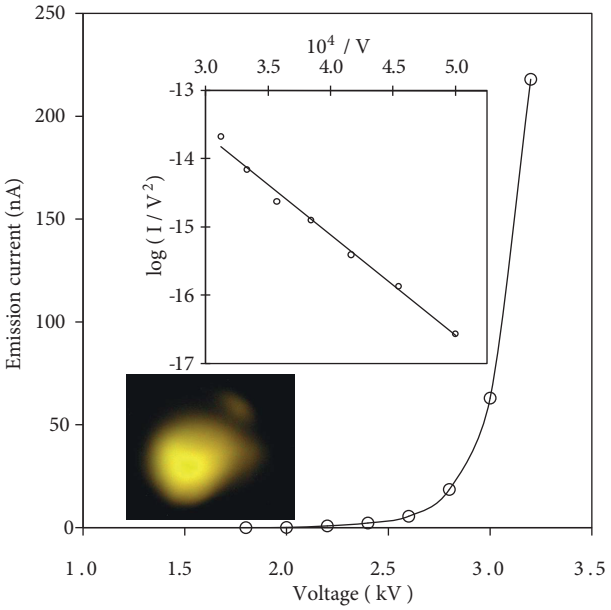

Figure 8. Field emission pattern, current–voltage characteristics, and corresponding FN plot obtained from LaB_6 nanoprotrusions.

Measurement of the TEDs was achieved for electrons emitting from the big protrusion. Mechanical manipulation of the emitter position was performed to project the bigger spot pattern on the probe hole of the anode. The anode was set to a few kilovolts and the V_L/V_A ratio was set to 0.0042. The sweeping rate of the emitter bias and the record rate of the collector current were 83.33 mV Hz and 5 Hz, respectively. Consecutive sweeps of the retarding curves were recorded through the picoammeter by a data-acquisition device and transferred to a computer for numeric processing. Retarding curves exhibiting atypical features and unpredictable fluctuations of higher than 15% in the readings of measurements could be omitted. Figure 9 shows 6 consecutive signal curves drawn from the LaB_6 nanoprotrusion. Averaging over multiple identical sweeps was performed before the first derivative was determined by numerical differentiation. The TEDs were normalized to peak value and to the work function of the collector. Figure 10 shows the retarding curve and the corresponding TED of the field-emitted electrons from the big protrusion of the LaB_6/W emitter. The TED exhibits a single peak located near the Fermi energy of the metallic emitter indicating a significant potential deformation at the surface of the emitter and insignificant potential drop inside the material. The peak position is found independent of the anode bias (i.e. no peak shift), verifying a metallic behavior of the LaB_6/W cathode where field penetration is negligibly small due to the high density of electrons at its surface. The slope of the high-energy side of the peak is lower than that of the low-energy side, where the distribution is said to exhibit a tail feature. The higher slope is due to the exponential increase of the tunneling probability near the Fermi level. The tail feature is due to the decrease of the density of occupied states below the Fermi level of the metallic material. The best FWHM of the TEDs is 0.3 eV. The relative resolution of the analyzer has been determined as 0.068.

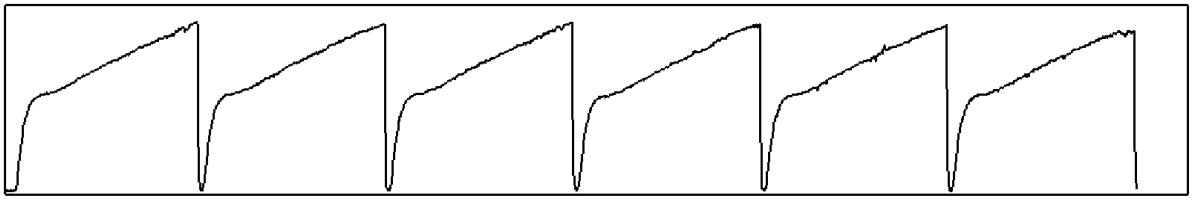

Figure 9. Consecutive sweeps of retarding curves obtained from the retarding analyzer.

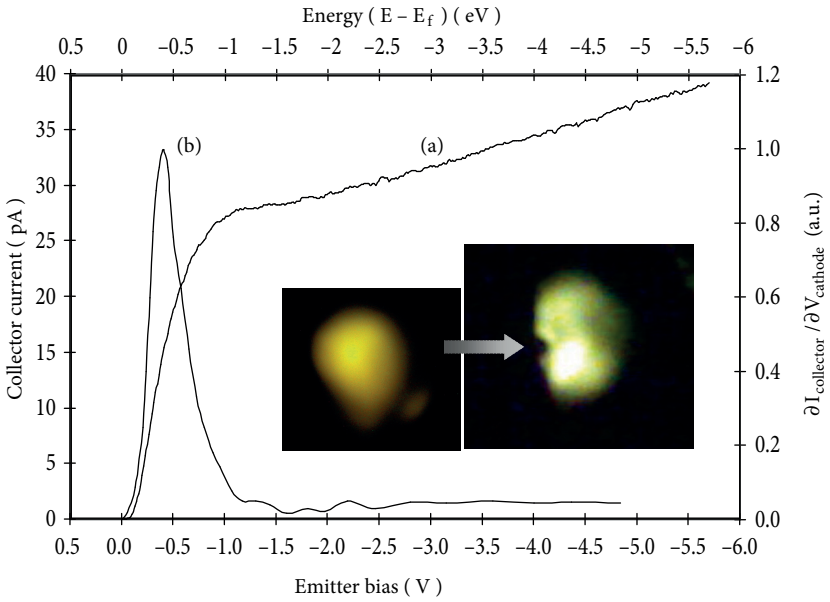

Figure 10. Retarding curve (a) and corresponding TED (b) of LaB_6/W. Inset: Electron emission pattern projected on anode of the analyzer (the arrow points to the anode probe hole).

The field emission characteristics of the LaB_6/W, being consistent with the FN theory, suggest that no size effects occur despite electrons' emission from protrusions of a few hundred nanometers (within 300 nm in radius in the present case). The linear characteristic of the FN plot and the single non-broadened feature of the TEDs clarify that quantum effects due to small sizes of the emitters are not significant. These effects would otherwise be observed for sharper emitters as deviation from linearity in the FN plot accompanied with broadening and peak splitting in the TEDs [22,23]. Therefore, bulk properties are being observed. It is beyond the scope of this paper to deal with the modifications and corrections of the FN theory and their manifestation in the measurements. Forbes introduced sophisticated treatments of this aspect (see, for example, [24–26]).

4. Conclusions

A simple configuration of a retarding analyzer has been optimized, calibrated, and successfully used for field emission investigation. Both basic current–voltage characteristics and quantitative total energy distribution measurements could be simultaneously achieved with high-accuracy and low-cost instrumentation. The direct detection technique, averaging over consecutive measurements, and numerical differentiation of output signal were also adopted to address the presumed shortages of sophisticated instrumental requirements for field emission investigation. Electron emission from LaB_6 nanoprotrusions, deposited on a clean tungsten microtip, was

investigated satisfactorily and the results emphasized the metallic behavior of the emitter in accordance with FN theory. No size effects were observed for protrusions of 300 nm in radii, suggesting that these were not sharp emitters.

References

[1] T. Yoshida, H. Naito, M. Okuda, S. Ehara, T. Takagi, O. Kusumoto, H. Kado, K. Yokoyama and T. Tohda, *Appl. Phys. Lett.*, **64**, (1994), 3243.

[2] Q. Wan, K. Yu, T. H. Wang and C. L. Lin, *Appl. Phys. Lett.*, **83**, (2003), 2253.

[3] N. S. Ramgir, I. S. Mulla, K. Vijayamohanan, D. J. Late, A. B. Bhise, M. A. More and D. S. Joag, *Appl. Phys. Lett.*, **88**, (2006), 042107.

[4] H. Zhang, J. Tang, Q. Zhang, G. Zhao, G. Yang, J. Zhang, O. Zhou and L. Qin, *Adv. Mater.*, **18**, (2006), 87.

[5] A. G. J. Van Oostrom, *Philips Res. Rep.*, Suppl. **1**, (1966), 49.

[6] N. de Jonge, Y. Lamy, K. Schoots, T. H. Oosterkamp, *Nature*, **420**, (2002), 393.

[7] J. Zhang, J. Tang, G. Yang, Q. Qiu, L. C. Qin and O. Zhou, *Adv. Mater.*, **16**, (2004), 1219.

[8] N. de Jonge, J. M. Bonard, *Phil. Trans. R. Soc. Lond.*, **A362**, (2004), 2239.

[9] R. H. Fowler and L. W. Nordheim, *Proc. Roy. Soc. (London)*, **A119**, (1928), 173.

[10] R. D. Young, *Phys. Rev.*, **113**, (1959), 110.

[11] J. W. Gadzuk and E. W. Plummer, *Rev. Mod. Phys.*, **45**, (1973), 487.

[12] R. D. Young and C. E. Kuyatt, *Rev. Sci. Instrum.*, **39**, (1968), 1477.

[13] R. V. Latham and M. S. Mousa, *J. Phys. D: Appl. Phys.*, **19**, (1986), 699.

[14] L. Marton and J. A. Simpson, *Rev. Sci. Instrum.*, **29**, (1958), 567.

[15] H. G. Noller, H. D. Polaschegg and H. Schillalies, *J. Elect. Spectrosc. Relat. Phenom.*, **5**, (1974), 705.

[16] A. W. Blackstock, R. D. Birkhoff, and M. Slater, *Rev. Sci. Instrum.*, **26**, (1955), 274.

[17] D. Roy and J. D. Carrette, *Rev. Sci. Instrum.*, **42**, (1971), 1122.

[18] M. E. Rudd, Low Energy Electron Spectrometry (Wiley-Interscience, New York. 1972), p. 7.

[19] L. B. Leder and J. A. Simpson, *Rev. Sci. Instrum.*, **29**, (1958), 571.

[20] W. M. Mulaire and W. T. Peria, *Surf. Sci.*, **26**, (1971), 125.

[21] D. J. Late, M. A. More, D. S. Joag, P. Misra, B. N. Singh and L. M. Kukreja, *Appl. Phys. Lett.*, **89**, (2006), 123510.

[22] K. S. Yeong and J. T. L. Thong, *J. Appl. Phys.*, **100**, (2006), 114325.

[23] M. L. Yu and T. H. P. Chang, *Appl. Surf. Sci.*, 146, (1999), 334.

[24] R. G. Forbes, *Nanotechnology*, **23**, (2012), 095706.

[25] R. G. Forbes, *J. Vac. Sci. Technol. B.*, **26**, (2008), 788.

[26] R. G. Forbes, *J. Appl. Phys.*, **104**, (2008), 084303.